

# Ocean currents show global intensification of weak tropical cyclones

<https://doi.org/10.1038/s41586-022-05326-4>

Guihua Wang<sup>1,4</sup>✉, Lingwei Wu<sup>1,4</sup>, Wei Mei<sup>2</sup> & Shang-Ping Xie<sup>3</sup>

Received: 18 February 2022

Accepted: 6 September 2022

Published online: 16 November 2022

 Check for updates

Theory<sup>1</sup> and numerical modelling<sup>2</sup> suggest that tropical cyclones (TCs) will strengthen with rising ocean temperatures. Even though models have reached broad agreement on projected TC intensification<sup>3–5</sup>, observed trends in TC intensity remain inconclusive and under active debate<sup>6–10</sup> in all ocean basins except the North Atlantic, where aircraft reconnaissance data greatly reduce uncertainties<sup>11</sup>. The conventional satellite-based estimates are not accurate enough to ascertain the trend in TC intensity<sup>6,11</sup>, suffering from contamination by heavy rain, clouds, breaking waves and spray<sup>12</sup>. Here we show that weak TCs (that is, tropical storms to category-1 TCs based on the Saffir–Simpson scale) have intensified in all ocean basins during the period 1991–2020, based on huge amounts of highly accurate ocean current data derived from surface drifters. These drifters have submerged ‘holy sock’ drogues at 15 m depth to reduce biases induced by processes at the air–sea interface and thereby accurately measure near-surface currents, even under the most destructive TCs. The ocean current speeds show a robust upward trend of ~4.0 cm s<sup>-1</sup> per decade globally, corresponding to a positive trend of 1.8 m s<sup>-1</sup> per decade in the TC intensity. Our analysis further indicates that globally TCs have strengthened across the entirety of the intensity distribution. These results serve as a historical baseline that is crucial for assessing model physics, simulations and projections given the failure of state-of-the-art climate models in fully replicating these trends<sup>13</sup>.

In addition to their tremendously destructive impacts on economy and society, TCs play an important role in the atmosphere–ocean system<sup>14–18</sup>. TC intensity is often defined using the 1 min, 2 min or 10 min maximum sustained surface wind speed at 10 m height. However, this parameter is not only notoriously difficult to predict, but also extremely hard to accurately estimate from observations<sup>19</sup>. The Dvorak technique is an empirical method widely used for estimating TC intensity from satellite imagery<sup>20,21</sup>. In practice, this technique first estimates a final T number (FT) from cloud patterns and infrared cloud top temperatures, then obtains a current intensity number (CI) from FT based on several rules and finally converts CI to maximum sustained wind (MSW) using a standard table. Because of the subjectiveness of the FT estimates, CI assignment and differences in the conversion table in use, the intensity estimates by different agencies can vary a lot even based on identical information<sup>22</sup> (Extended Data Table 1), especially for 1 min maximum wind speeds below 90 kt and above 125 kt (ref. <sup>23</sup>). Consequently, TC intensities in the ‘best track’ dataset obtained using this subjective technique have large uncertainties for trend analysis. The study in ref. <sup>24</sup> concluded that the total destructiveness of TCs have increased markedly over a period of 30 years starting in the mid-1970s. Based on peak intensity during a TC lifetime, the research of ref. <sup>25</sup> suggested that the upward trend in intensity only occurs to strong TCs (that is, categories 3–5) but not to weak TCs. It has also been found<sup>26</sup> that the strongest TCs (that is, categories 4–5) had increased from 1970 to 2004 in all

basins except the North Atlantic. Using a new satellite-based dataset, it has been found<sup>27</sup> that the proportion of strong TCs increased during the period 1975–2010, whereas it has been suggested<sup>28</sup> that the global mean trend in TC intensity over the period 1982–2009 is statistically insignificant. Observed estimates of trends in TC intensity have not converged and the uncertainty remains large<sup>3,11,29</sup>. Here we develop a new approach to evaluate the changes in TC intensity during the last three decades by using huge amounts of surface drifter-derived ocean current data with high accuracy.

A close relationship between TCs and ocean currents has been identified from ocean dynamics<sup>30</sup>, verified by various observations including acoustic Doppler current profilers<sup>31</sup>, air-borne expendable current profilers<sup>32</sup>, moored and drifting buoys<sup>33</sup>, electromagnetic autonomous profiling explorer floats<sup>34</sup> and surface drifters<sup>35</sup>. Although anemometers fail to function when the air–sea boundary is not well defined, surface drifters are equipped with a drogue for nominal 15 m currents and are not strongly biased by processes at the air–sea interface (for example, winds and breaking waves). Robust evidence has been provided<sup>36</sup> for the near-surface current response to TCs from tropical storms to category-5 TCs. This suggests that ocean current observations can provide alternative estimates of TC intensity, given the large amounts of direct near-surface current measurements by surface drifters. Over 25,000 drifters have been deployed globally since the start of the National Oceanic and Atmospheric Administration Global Drifter Program in 1979,

<sup>1</sup>Department of Atmospheric and Oceanic Sciences and CMA-FDU Joint Laboratory of Marine Meteorology, Fudan University, Shanghai, China. <sup>2</sup>Department of Earth, Marine and Environmental Sciences, University of North Carolina at Chapel Hill, Chapel Hill, NC, USA. <sup>3</sup>Scripps Institution of Oceanography, University of California San Diego, La Jolla, CA, USA. <sup>4</sup>These authors contributed equally: Guihua Wang, Lingwei Wu. ✉e-mail: wanggh@fudan.edu.cn

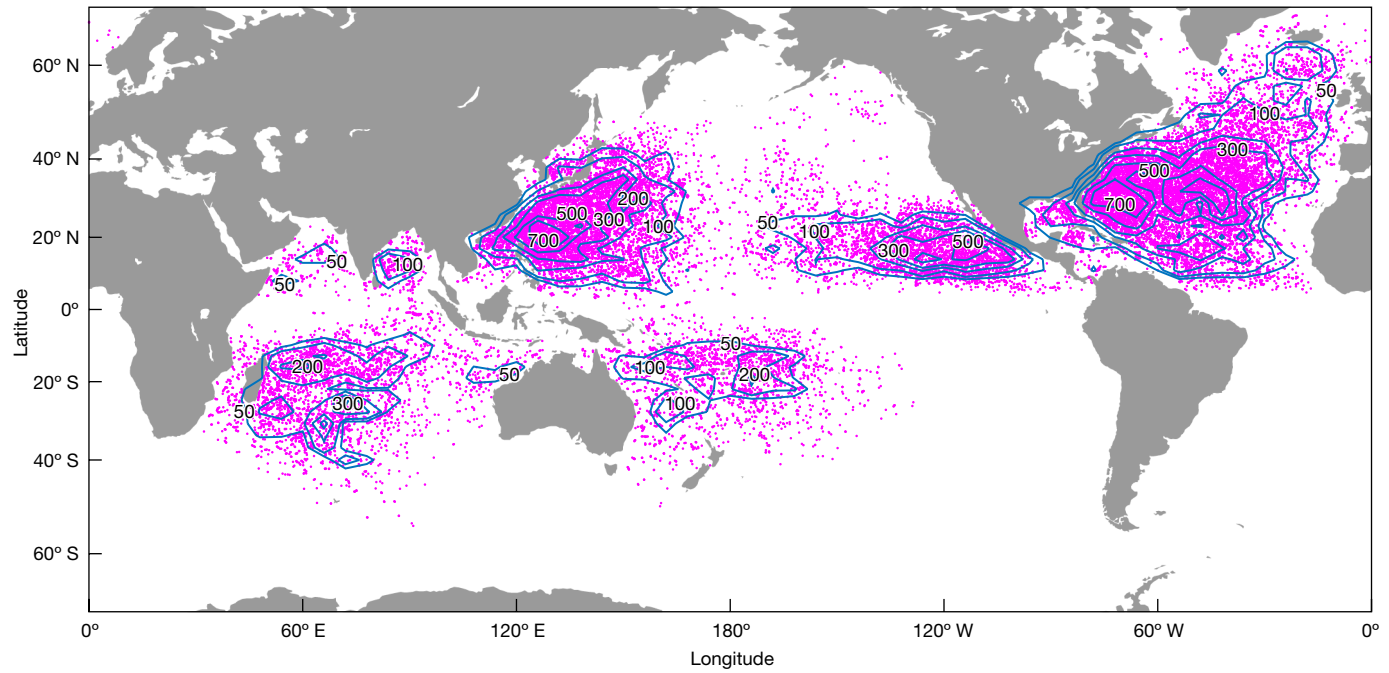


**Fig. 1 | Data distribution.** Data points of drifters (pink dots) that are located within a distance from the TC centre of  $r < 7R_{\max}$  under weak TC conditions and the number of corresponding weak TC centres in a  $6^\circ \times 3^\circ$  grid box (blue

contours of 50, 100, 200, 300, 500 and 700) during the period 1991–2020. The total number of drifter records is 85,411. This figure is produced using MATLAB.

and more than 36 million records of measurements are available. More importantly, these ocean current measurements are of high accuracy: for a  $10 \text{ m s}^{-1}$  wind speed, the downwind bias in the measured ocean currents is only around  $1 \text{ cm s}^{-1}$  (ref. <sup>37</sup>), corresponding to an error in wind speed of approximately  $0.46 \text{ m s}^{-1}$  based on Ekman theory. The wind speed of TCs inferred from the drifter current measurements is highly consistent with the observed wind speed from global tropical buoy arrays, with a root mean square error of  $2 \text{ m s}^{-1}$  (Methods and Extended Data Fig. 1b). Thus, it is viable to quantify the trend in TC intensity using ocean current measurements from drifters.

There are more than 85,000 drifter records associated with weak TCs (defined as TCs of 1 min maximum sustained wind speed ranging between  $17$  and  $42 \text{ m s}^{-1}$  at the time of measurement), whereas much fewer drifter records (5,800) are available for strong TCs. It is important to ensure that the amount of drifter observations is sufficient to analyse the trend in TC intensity by compositing TC wind fields over different time periods. Adopting the method of ten events per variable (EPV) as a minimal criterion in sample-size consideration (Methods), we confirm that the drifter records are enough to composite the wind field for weak TCs but not sufficient for strong TCs globally at this point. We focus on weak TCs for trend analysis. Although weak TCs account for 70% of all TCs, accurate estimates of their intensity are much more challenging with the Dvorak technique<sup>23</sup>. For every five-consecutive-year period during 1991–2020, we compare the composite TC winds with the theoretical TC winds based on the Batts typhoon wind field model<sup>38</sup> (Methods) and find little differences between them (that is, less than  $0.5 \text{ m s}^{-1}$ ) (Extended Data Fig. 2a). Specifically, although the number of drifter records in the first five years is small (7,165, with around 23% of them being in the last five years), the composite TC wind field still bears much resemblance to the theoretical TC wind field (Extended Data Fig. 2b). This demonstrates the usefulness and accuracy of the proposed approach in constructing the TC wind field and estimating the trend in TC intensity using drifter current measurements.

We then extract all the drifter records within seven radii of the maximum sustained wind speed ( $R_{\max}$ ) of each weak TC from 1991 to 2020 (Fig. 1), and construct the composite ocean current fields for weak TCs

for each ocean basin in individual years. The total number of records is 38,318, 12,262, 20,568, 8,000 and 4,962 in the North Atlantic Ocean (NA), Northeast Pacific Ocean (NEP), Northwest Pacific Ocean (NWP), South Indian Ocean (SI) and South Pacific Ocean (SP), respectively. The North Indian Ocean (NI) is not well sampled under weak TC conditions (only 1,301 drifter records during the entire 30-year period) and hence is excluded in this study.

Figure 2 shows spatially averaged current speeds within seven  $R_{\max}$  associated with weak TCs for individual basins spanning the 30 years from 1991 to 2020, as well as for the globe (solid lines). It is evident that current speeds have notably increased over all ocean basins, with an upward trend of around  $0.40 \text{ cm s}^{-1}$  per year on a global scale. This upward trend is much stronger than the background trend of around  $0.15 \text{ cm s}^{-1}$  per year, which is calculated using all drifter observations and reflects the acceleration of global mean ocean circulation over the past three decades<sup>39</sup>. In individual basins, the trend is  $0.35$ ,  $0.29$ ,  $0.36$ ,  $0.39$  and  $0.54 \text{ cm s}^{-1}$  per year for the NA, NEP, NWP, SI and SP, respectively. We have repeated the computations using one to six  $R_{\max}$ , and obtained consistent results, which tend to show stronger upward trends in the mean current speed both globally and for individual basins (Extended Data Table 2).

Based on the relationship between ocean surface Ekman current speed and wind speed at  $10 \text{ m}$  height (Methods), we estimate the trend in the intensity of weak TCs to be  $0.18 \text{ m s}^{-1}$  per year from the trend in global mean ocean current speed (that is,  $0.40 \text{ cm s}^{-1}$  per year) during the period 1991–2020. The estimated trend in the intensity of weak TCs is around 20% larger than the trend in the lifetime peak intensity of strong TCs revealed in ref. <sup>25</sup> ( $0.15 \text{ m s}^{-1}$  per year). Using the maximum wind speed obtained from the Batts typhoon wind field model<sup>38</sup> that incorporates drifter current measurements, we further estimate the destructiveness of weak TCs, calculated as the annually accumulated power dissipation index (PDI)<sup>24</sup>, and find a robust upward trend as well. These results are distinct from the weak downward trend inferred from available TC best track datasets (bottom panel of Fig. 2). Consistent with the PDI calculation, the probability density function (PDF) of the intensity of weak TCs derived from drifter observations also shifts to

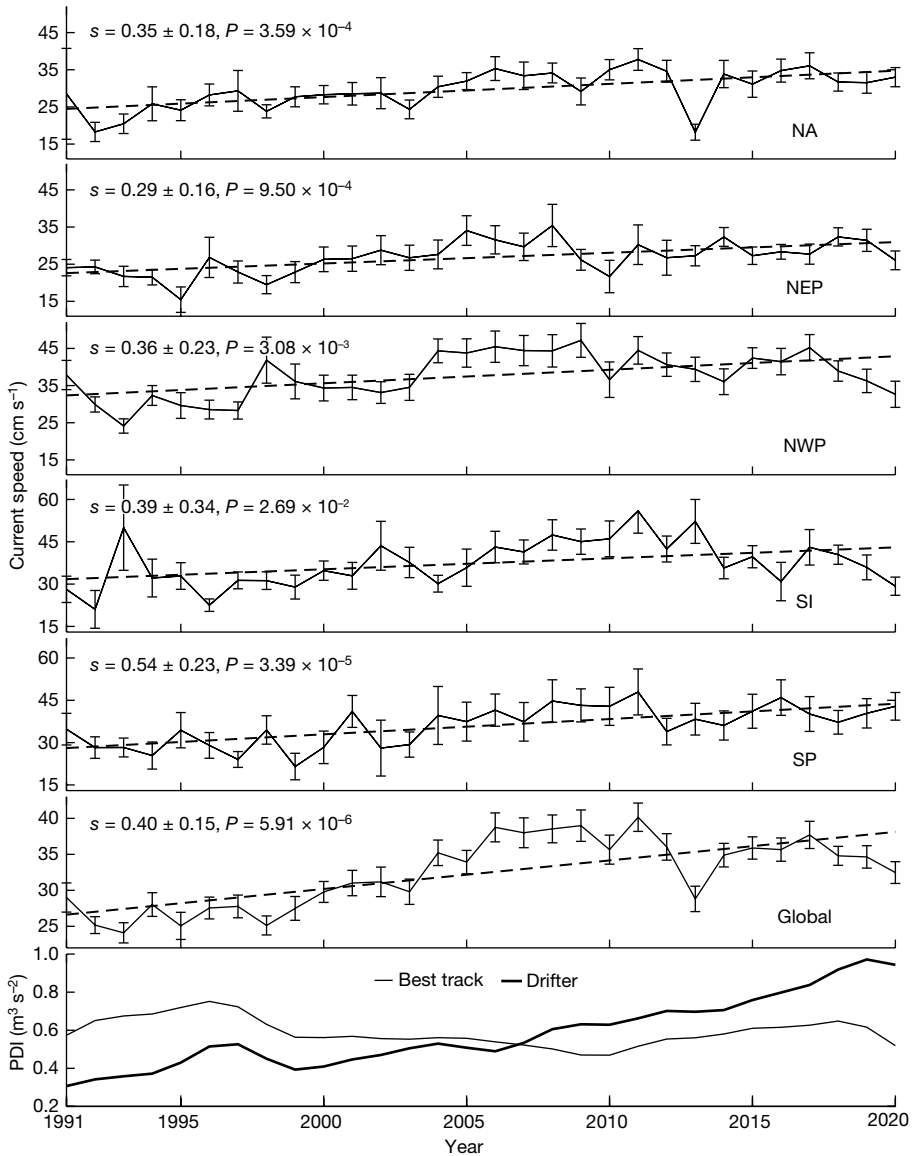


**Fig. 2 | Evolution of the near-surface ocean current speeds under weak TCs.**

Spatial averages of drifter-measured current speeds from 1991 to 2020 for individual basins and the globe (solid lines). Drifter records used for the calculation are shown in Fig. 1 as pink dots. In each panel, the dashed line indicates the fitted linear trend of the curve. The slope ( $s$ ) of the fitted line (along with the 95% margin of error) and the  $P$  value of the  $t$ -test for the trend are also reported. The length of the error bar for each year is twice the standard deviation divided by the square root of the effective number of observations in

that year (that is, twice the standard error of the mean). The effective number of observations is approximated as the number of observations that are separated by at least 500 km in distance or at least 10 days in time. In the bottom panel, the annually accumulated PDIs have been multiplied by  $0.9 \times 10^{-12}$ . The maximum wind speeds are from two datasets: the thin solid line is derived from the TC best track datasets and the thick solid line is derived from the drifter current measurements based on the Batt's typhoon wind field model.

higher intensities during the recent one and a half decades (Extended Data Fig. 3a). This PDF shift is independent of data sampling (Extended Data Fig. 3b), demonstrating that the rise of the TC intensity is robust across the 17–42 m s<sup>-1</sup> range.

Figure 3a compares the composites of global mean observed ocean currents and their standard error ellipses in the along-track and cross-track coordinate system under weak TCs during the periods of 1991–2005 and 2006–2020. The coherent spatial structure of TC-induced ocean circulation during both periods corroborates that the number of drifter measurements is sufficient to robustly estimate ocean currents under weak TCs (the number of drifter records is shown in Extended Data Fig. 4a). A strongly asymmetric TC-induced ocean circulation exists in both periods, and the epoch differences show a prominent cyclonic circulation anomaly, suggesting a strengthening of the TC-induced oceanic circulation from 1991–2005 to 2006–2020.

This result is nearly independent of whether the trend in the background current is removed or not as TC-induced currents are transient and rotational. Quantitatively, the ocean current speed maximum is approximately 29.9 cm s<sup>-1</sup> during the period 1991–2005 and increases by over 40% to around 42.4 cm s<sup>-1</sup> during the period 2006–2020. The coherent pattern of the circulation change provides further support for the intensification of weak TCs in recent decades. Consistently, our composite wind fields of weak TCs for the two periods based on drifter observations also show a comparable upward trend (Extended Data Fig. 2c). Moreover, our computations suggest that the upward trend is largest between one and two  $R_{\max}$  of TCs (Extended Data Fig. 5), in line with previous studies<sup>30</sup>. We further construct the composites of observed ocean currents under weak TCs for individual basins during the periods 1991–2005 and 2006–2020 (Fig. 3b). Notably, all the five basins show coherent cyclonic circulation anomalies from the first to

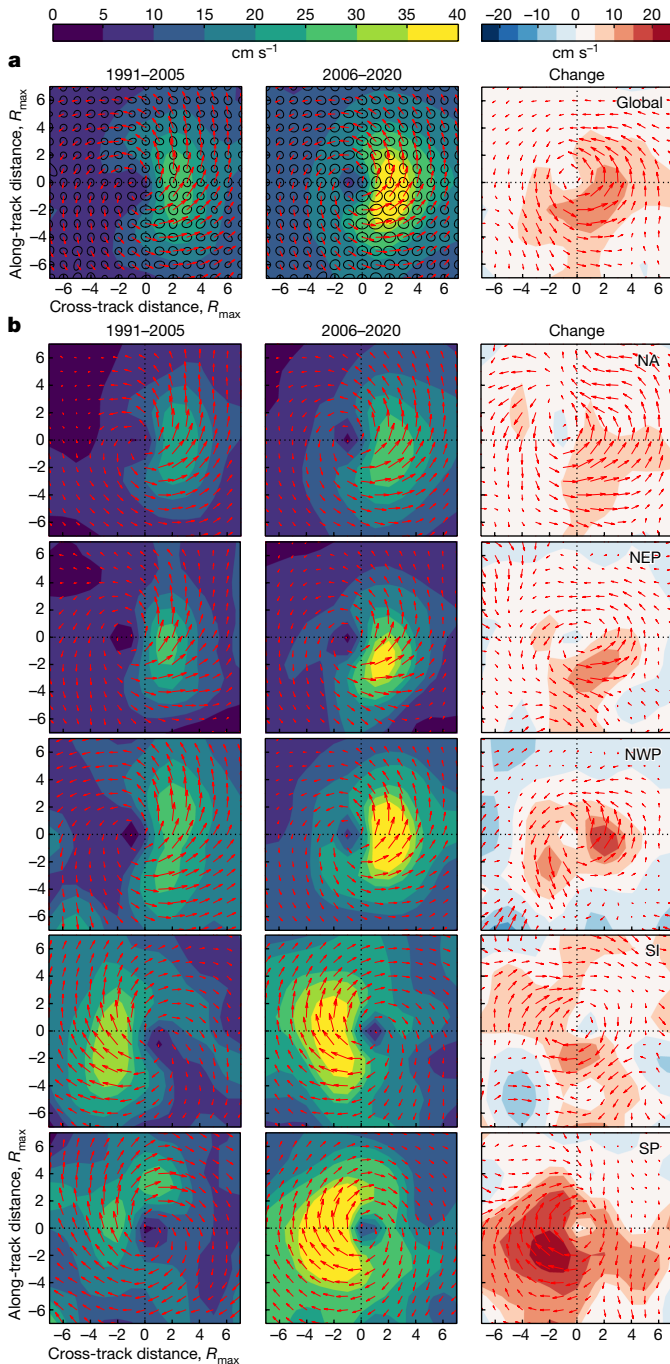


**Fig. 3 | Mean near-surface ocean current fields under weak TCs.** **a**, Global mean current fields for the periods 1991–2005 and 2006–2020, and the change of the mean currents between the two periods (2006–2020 minus 1991–2005). **b**, As in **a** but for five ocean basins.

second period. As listed in Table 1, the maximum and mean current speed increases are  $8.2/4.1$ ,  $11.4/3.2$ ,  $16.1/2.0$ ,  $7.4/4.4$  and  $21.8/9.0\text{ cm s}^{-1}$  for the NA, NEP, NWP, SI and SP, respectively. Globally, the mean current speed increases by around  $5.0\text{ cm s}^{-1}$ , corresponding to an increase of approximately  $2.3\text{ m s}^{-1}$  in the average wind speed.

To further test the robustness of our results, we repeated the analysis using the subset of storms with instantaneous maximum intensity of tropical storm strength ( $17\text{--}32\text{ m s}^{-1}$ ). The results show the intensity of TCs at tropical storm strength is also increasing for individual basins and globally (Extended Data Figs. 8a and 4e), reaffirming that the upward trend in TC intensity is robust. Everything else being equal,

**Table 1 | Statistics of drifter-measured ocean current speeds under weak TCs**

Basin	1991–2005	2006–2020	Change
	Maximum/mean	Maximum/mean	Maximum/mean
NA	24.1/9.9	32.3/14.0	8.2/4.1
NEP	27.6/10.5	39.0/13.7	11.4/3.2
NWP	30.8/16.3	46.9/18.3	16.1/2.0
SI	38.1/17.7	45.5/22.1	7.4/4.4
SP	29.8/16.4	51.6/25.4	21.8/9.0
Global	29.9/14.3	42.4/19.3	12.5/5.0

All units are  $\text{cm s}^{-1}$ . The change means the maximum/mean ocean current speeds under weak TCs of the period 2006–2020 minus those of 1991–2005.

stronger TCs induce more intense surface cooling. Figure 4 shows the composite sea surface cooling produced by weak TCs for the two time periods, calculated in the same way as for the global mean ocean currents. The maximum cooling within  $r < 7R_{\max}$  is about  $-0.27\text{ }^{\circ}\text{C}$  and  $-0.36\text{ }^{\circ}\text{C}$  for the periods 1991–2005 and 2006–2020, respectively. The enhanced sea surface cooling in the later period is largely attributed to the intensification of weak TCs after ruling out other potentially important factors<sup>39,40</sup>: the translational speed of weak TCs did not change much (Extended Data Fig. 6); upper-ocean stratification<sup>41</sup> increase is modest; and the mixed layer depth decrease is insignificant (Extended Data Fig. 7c,d).

Our analysis so far concerns the intensity at the time of drifter measurements, whereas in the literature weak TCs often refer to storms with lifetime maximum intensity (LMI) of  $17\text{--}42\text{ m s}^{-1}$ . Therefore, we constructed another two subsets, one for storms with LMI at tropical storm (TS) strength ( $17\text{--}32\text{ m s}^{-1}$ ) and the other for storms with LMI of TS to category-1 strength ( $17\text{--}42\text{ m s}^{-1}$ ). The drifter-derived ocean current speeds for both subsets show upward trends for individual basins and globally (Extended Data Figs. 8b,c and 4f,g), which are comparable and consistent with those shown in Fig. 2 and Fig. 3a. All these results show that weak TCs have become stronger over the recent three decades, regardless of whether the time for which an intense storm is weak is included or not.

In summary, both drifter current observations and satellite-based TC-induced sea surface cooling demonstrate that weak TCs have intensified in recent decades. This is distinct from the change inferred from the traditional best track datasets that show the intensification of only strong TCs. The increase in the intensity of weak TCs is in line with the observed trends in the large-scale atmospheric environment in which TCs develop, particularly the thermodynamic fields (that is, potential intensity and mid-tropospheric relative humidity; Extended Data Fig. 7a,b). The contribution of the changes in upper-ocean thermal stratification<sup>42</sup> is rather modest (Extended Data Fig. 7c). The observed intensification of weak TCs is not simulated by state-of-the-art climate models<sup>13</sup>, challenging current model physics and projections. Because the vast majority of TCs are in the weak category, our finding that weak TCs have intensified could aid model improvement and TC projections. Most importantly, we present an alternative accurate method to estimate TC intensity in remote oceans. At this stage, available drifter data limit our detection of global TC intensification to the wind speed range of  $17\text{--}42\text{ m s}^{-1}$ , but the change in TC intensity PDF (Extended Data Fig. 3) seems to imply an overall shift towards higher intensities globally. Over the NWP, the only basin with sufficient drifter data, ocean current speeds for strong TCs show an upward trend of around  $0.6\text{ cm s}^{-1}$  per year (Extended Data Fig. 8d). With more drifter data accumulating over time, our method has the potential to reveal the full spectral change in TC intensity. Observing and identifying such spectral changes in TC intensity are important, both in their own right and for testing high-resolution models.

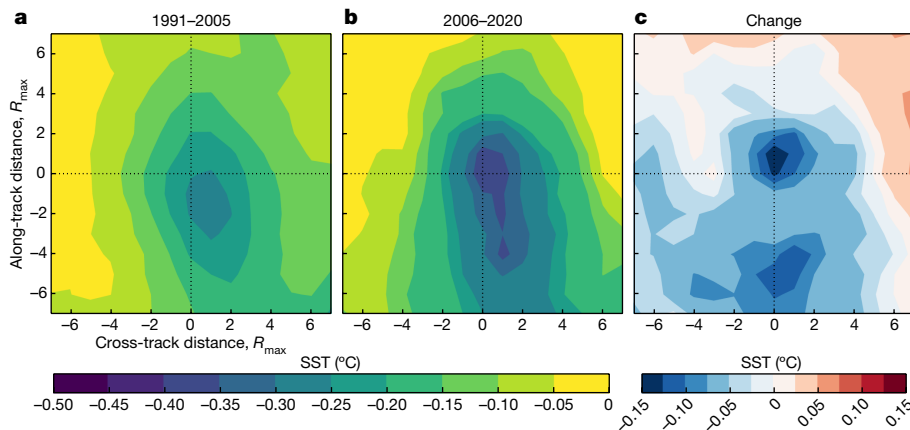


**Fig. 4 | Sea surface cooling induced by weak TCs.** **a–c**, Sea surface temperature (SST) anomalies induced by weak TCs for the periods of 1991–2005 (**a**) and 2006–2020 (**b**), as well as change of the SST anomalies between the two periods (2006–2020 minus 1991–2005) (**c**).

## Online content

Any methods, additional references, Nature Research reporting summaries, source data, extended data, supplementary information, acknowledgements, peer review information; details of author contributions and competing interests; and statements of data and code availability are available at <https://doi.org/10.1038/s41586-022-05326-4>.

- Emanuel, K. A. The dependence of hurricane intensity on climate. *Nature* **326**, 483–485 (1987).
- Knutson, T. R. & Tuleya, R. E. Impact of CO<sub>2</sub>-induced warming on simulated hurricane intensity and precipitation: Sensitivity to the choice of climate model and convective parameterization. *J. Clim.* **17**, 3477–3495 (2004).
- Sobel, A. et al. Human influence on tropical cyclone intensity. *Science* **353**, 242–246 (2016).
- Emanuel, K. Response of global tropical cyclone activity to increasing CO<sub>2</sub>: results from downscaling CMIP6 models. *J. Clim.* **34**, 57–70 (2021).
- Knutson, T. et al. Tropical cyclones and climate change assessment: Part II: projected response to anthropogenic warming. *Bull. Amer. Meteor. Soc.* **101**, E303–E322 (2020).
- Landsea, C. W. Hurricanes and global warming. *Nature* **438**, E11–E13 (2005).
- Pielke, R. A. Are there trends in hurricane destruction? *Nature* **438**, E11 (2005).
- Knutson, T. et al. Tropical cyclones and climate change assessment: Part I: detection and attribution. *Bull. Amer. Meteor. Soc.* **100**, 1987–2007 (2019).
- Klotzbach, P. et al. Trends in global tropical cyclone activity: 1990–2021. *Geophys. Res. Lett.* **49**, e2021GL095774 (2022).
- Schreck, C. J. III, Knapp, K. R. & Kossin, J. P. The impact of best track discrepancies on global tropical cyclone climatologies using IBTrACS. *Mon. Weather Rev.* **142**, 3881–3899 (2014).
- Hennon, C. et al. Cyclone center: can citizen scientists improve tropical cyclone intensity records? *Bull. Amer. Meteor. Soc.* **96**, 591–607 (2015).
- Weissman, D. E., Bourassa, M. A. & Tongue, J. Effects of rain rate and wind magnitude on sea winds scatterometer wind speed errors. *J. Atmos. Oceanic Technol.* **19**, 738–746 (2002).
- Jing, R., Lin, N., Emanuel, K., Vecchi, G. & Knutson, T. R. A comparison of tropical cyclone projections in a high-resolution global climate model and from downscaling by statistical and statistical-deterministic methods. *J. Clim.* **34**, 9349–9364 (2021).
- Emanuel, K. Contribution of tropical cyclone to meridional heat transport by the oceans. *J. Geophys. Res.* **106**, 14771–14781 (2001).
- Lin, I. et al. The interaction of Supertyphoon Maemi (2003) with a warm ocean eddy. *Mon. Weather Rev.* **133**, 2635–2649 (2005).
- Sriver, R. & Huber, M. Observational evidence for an ocean heat pump induced by tropical cyclones. *Nature* **447**, 577–580 (2007).
- Korty, R. L., Emanuel, K. A. & Scott, J. R. Tropical cyclone-induced upper-ocean mixing and climate: application to equitable climates. *J. Clim.* **21**, 638–654 (2008).
- Zhang, Y., Zhang, Z., Chen, D., Qiu, B. & Wang, W. Strengthening of the Kuroshio current by intensifying tropical cyclones. *Science* **368**, 988–993 (2020).
- DeMaria, M., Sampson, C. R., Knaff, J. A. & Musgrave, K. D. Is tropical cyclone intensity guidance improving? *Bull. Amer. Meteor. Soc.* **95**, 387–398 (2014).
- Dvorak, V. F. Tropical cyclone intensity analysis and forecasting from satellite imagery. *Mon. Weather Rev.* **103**, 420 (1975).
- Dvorak, V. F. Tropical cyclone intensity analysis using satellite data. *NOAA Tech. Rep. NESDIS* **11**, 47 (1984).
- Landsea, C. W., Harper, B. A., Hoarau, K. & Knaff, J. A. Can we detect trends in extreme tropical cyclones? *Science* **313**, 452–454 (2006).
- Knaff, J. A., Brown, D. P., Courtney, J., Gallina, G. M. & Beven, J. L. An evaluation of Dvorak technique-based tropical cyclone intensity estimates. *Weather Forecast.* **25**, 1362–1379 (2010).
- Emanuel, K. A. Increasing destructiveness of tropical cyclones over the past 30 years. *Nature* **436**, 686–688 (2005).
- Elsner, J. B., Kossin, J. P. & Jagger, T. H. The increasing intensity of the strongest tropical cyclones. *Nature* **455**, 92–95 (2008).
- Webster, P. J., Holland, G. J., Curry, J. A. & Chang, H.-R. Changes in tropical cyclone number, duration, and intensity in a warming environment. *Science* **309**, 1844–1846 (2005).
- Holland, G. & Bruyère, C. L. Recent intense hurricane response to global climate change. *Clim. Dyn.* **42**, 617–627 (2014).
- Kossin, J. P., Olander, T. L. & Knapp, K. R. Trend analysis with a new global record of tropical cyclone intensity. *J. Clim.* **26**, 9960–9976 (2013).
- Kossin, J. P., Knapp, K. R., Olander, T. L. & Velden, C. S. Global increase in major tropical cyclone exceedance probability over the past four decades. *Proc. Natl. Acad. Sci.* **117**, 11975–11980 (2020).
- Price, J. F., Sanford, T. B. & Forristall, G. Z. Forced stage response to a moving hurricane. *J. Phys. Oceanogr.* **24**, 233–260 (1994).
- Pallás-Sanz, E., Candela, J., Sheinbaum, J. & Ochoa, J. Mooring observations of the near-inertial wave wake of Hurricane Ida (2009). *Dyn. Atmospheres Oceans* **76**, 325–344 (2016).
- Sanabria, E. R. & Jayne, S. R. Ocean observations under two major hurricanes: evolution of the response across the storm wakes. *AGU Advances* **1**, e2019AV000161 (2020).
- Li, R. et al. Slope-intensified storm-induced near-inertial oscillations in the South China Sea. *J. Geophys. Res. Oceans* **126**, e2020JC016713 (2021).
- Hsu, J.-Y., Lien, R. -C., D'Asaro, E. A. & Sanford, T. B. Scaling of drag coefficients under five tropical cyclones. *Geophys. Res. Lett.* **46**, 3349–3358 (2019).
- Fan, S. et al. Observed ocean surface winds and mixed layer currents under tropical cyclones: Asymmetric characteristics. *J. Geophys. Res. Oceans* **127**, e2021JC017991 (2022).
- Chang, Y. C., Chen, G. Y., Tseng, R. S., Centurioni, L. R. & Chu, P. C. Observed near-surface flows under all tropical cyclone intensity levels using drifters in the northwestern Pacific. *J. Geophys. Res.* **118**, 2367–2377 (2013).
- Niiler, P. P., Sybrandy, A. S., Bi, K., Poula, P. M. & Bitterman, D. Measurements of the water following capability of holey-sock and TRISTAR drifters. *Deep-Sea Res.* **42**, 1951–1964 (1995).
- Batts, M. E., Russell, L. R. & Simiu, E. Hurricane wind speeds in the United States. *J. Struct. Div.* **106**, 2001–2016 (1980).
- Peng, Q. et al. Surface warming-induced global acceleration of upper ocean currents. *Sci. Adv.* **8**, eabj8394 (2022).
- Huang, P., Lin, I. I., Chou, C. & Huang, R. H. Change in ocean subsurface environment to suppress tropical cyclone intensification under global warming. *Nat. Commun.* **6**, 7188 (2015).
- Mei, W. & Pasquero, C. Spatial and temporal characterization of sea surface temperature response to tropical cyclones. *J. Clim.* **26**, 3745–3765 (2013).
- Mei, W., Xie, S. P., Primeau, F., McWilliams, J. C. & Pasquero, C. Northwestern Pacific typhoon intensity controlled by changes in ocean temperatures. *Sci. Adv.* **1**, e1500014 (2015).

**Publisher's note** Springer Nature remains neutral with regard to jurisdictional claims in published maps and institutional affiliations.

Springer Nature or its licensor holds exclusive rights to this article under a publishing agreement with the author(s) or other rightsholder(s); author self-archiving of the accepted manuscript version of this article is solely governed by the terms of such publishing agreement and applicable law.

© The Author(s), under exclusive licence to Springer Nature Limited 2022

## Methods

### Relating near-surface current and surface wind using Ekman theory

Ocean surface Ekman current speed<sup>43</sup> follows  $V_0 = \frac{\tau}{\sqrt{\rho_w f A_z}}$ , where  $\tau$  is the wind stress,  $\rho_w$  the density of sea water,  $f$  the Coriolis parameter and  $A_z$  the eddy viscosity coefficient. Furthermore, it can be reduced to  $V_0 = \frac{0.0127}{\sqrt{\sin |\varphi|}} U_{10}$ , where  $\varphi$  is the latitude ( $|\varphi| \geq 10^\circ$ ) and  $U_{10}$  the wind speed at 10 m height, on the basis of a bulk formula of  $\tau$  ( $\tau = \rho_{air} C_d U_{10}^2$ , where  $\rho_{air}$  is the density of air and  $C_d$  is the drag coefficient) and historical in situ observations. Therefore,  $U_{10}$  can be estimated from  $U_{10} = \frac{V_0 \times \sqrt{\sin |\varphi|}}{0.0127}$  with knowledge of the ocean surface Ekman current speed  $V_0$  (daily ocean surface geostrophic current climatology is removed). Here  $C_d$  is set to  $2.6 \times 10^{-3}$  unless specified otherwise. The drag coefficient  $C_d$  under high-wind conditions is neither well understood nor measured. The above current to wind conversion is meant to be advisory as TC intensity is traditionally defined in wind speed. We have tested our results using two formulae of  $C_d$  following refs. <sup>44,45</sup>, respectively:

$$C_{d1} = \begin{cases} (0.8 + 0.065U_{10}) \times 10^{-3}, & U_{10} \leq 31.5 \text{ m s}^{-1} \\ \left[ 0.55 + 2.97 \left( \frac{U_{10}}{31.5} \right) - 1.49 \left( \frac{U_{10}}{31.5} \right)^2 \right] \times 10^{-3}, & U_{10} > 31.5 \text{ m s}^{-1} \end{cases}$$

$$C_{d2} = \begin{cases} (-0.016U_{10}^2 + 0.967U_{10} + 8.058) \times 10^{-4}, & U_{10} \leq 35 \text{ m s}^{-1} \\ 2.23 \times 10^{-3} \left( \frac{U_{10}}{35} \right)^{-1}, & U_{10} > 35 \text{ m s}^{-1} \end{cases}$$

The trend in global average wind is  $0.16 \text{ m s}^{-1}$  per year for both  $C_{d1}$  and  $C_{d2}$ , in comparison with  $0.18 \text{ m s}^{-1}$  per year using  $C_d = 2.6 \times 10^{-3}$ . The difference in wind speed between the two periods (2006–2020 versus 1991–2005) is  $2.0$  and  $1.9 \text{ m s}^{-1}$  for  $C_{d1}$  and  $C_{d2}$ , respectively, which is close to our calculation ( $2.3 \text{ m s}^{-1}$ ) with constant  $C_d$ .

### Relationship between near-surface current and surface wind in buoy observations

Nine moored buoys from the Research Moored Array for African-Asian-Australian Monsoon Analysis and Prediction (RAMA), the Tropical Atmosphere Ocean/Triangle Trans-Ocean Buoy Network (TAO/TRITON) and Prediction and Research Moored Array in the Tropical Atlantic (PIRATA) are used to evaluate the relationship between wind and current speeds. Four are located at ( $12^\circ$  S,  $67^\circ$  E), ( $8^\circ$  S,  $67^\circ$  E), ( $8^\circ$  S,  $95^\circ$  E), ( $12^\circ$  N,  $90^\circ$  E) in the Indian Ocean. Three are located at ( $8^\circ$  N,  $130^\circ$  E), ( $8^\circ$  N,  $137^\circ$  E), ( $8^\circ$  N,  $156^\circ$  E) in the NWP. Two are located at ( $12^\circ$  N,  $23^\circ$  W) and ( $20^\circ$  N,  $38^\circ$  W) in the NA. These buoys are influenced by TCs for a total of 1,533 times, namely, they have 1,533 h of wind and current observations under TCs in the period from July 2001 to December 2019. Generally, the wind speed increases with the current speed in buoy observations (Extended Data Fig. 1a). Based on Ekman theory, we derive the wind speed from the buoy current speed. The theoretical wind speed ranges from 1 to  $23 \text{ m s}^{-1}$ , and agrees well with the corresponding buoy wind speed, as shown in Extended Data Fig. 1b. The root mean square error of the theoretical wind speed from buoy wind speed is only around  $2 \text{ m s}^{-1}$ . Note that few observations (only 125 out of 1,533) are located within  $r < R_{max}$  of TCs, and these TCs are of relatively weak intensities (Extended Data Fig. 1c) with the buoy wind speed smaller than  $25 \text{ m s}^{-1}$ .

### Constructions of the theoretical and composite TC wind fields based on the typhoon wind field model of Batts

The following steps are taken to obtain the theoretical and composite TC wind fields. Step 1: estimate the trend of drifter-measured near-surface ocean current speed within  $r < 7R_{max}$  of weak TCs dur-

ing the period 1991–2020. Step 2: derive the trend of wind speed at 10 m height based on Ekman theory from the trend of near-surface ocean current speed. Step 3: construct two wind fields based on the typhoon wind field model of Batts<sup>38</sup> using the trend of wind speed. One is pure theoretical wind, for which only the pressure difference between the TC centre and periphery estimated from the trend of wind speed is considered during each five-consecutive-year period. The other is composite wind, for which only wind vectors at drifter locations are extracted. Step 4: compare the composite wind with the theoretical one. Small differences between them suggest that our composition method works well. Step 5: construct the composite wind fields from drifters for the two time periods of 1991–2005 and 2006–2020.

### EPV method for sample-size considerations

Ten EPV is a widely advocated minimal criterion for sample-size considerations in logistic regression analysis<sup>46</sup>. In idealized typhoon wind structure, the maximum wind can be estimated by the wind speed at a given location as both the radial decay factor and  $R_{max}$  are set. Thus the minimum sampling size is determined by  $\frac{\text{EPV value} \times \text{total TC records}}{\text{sampling TC records}}$  each year (EPV = 10 for this study). The minimum sampling size ranges from 11 to 116 (13 to 760) with a mean value of 28 (97) for composite maps of weak (strong) TCs. Based on the above criteria, drifter samples are enough for all basins except NI in the weak TC intensity range, but only NWP meets the criteria for strong TCs.

### Trends in the large-scale atmospheric environment and upper-ocean thermal stratifications

Monthly atmospheric variables (including sea level pressure, specific and relative humidity, temperature, and zonal and meridional winds) and SST from the Japanese 55-year Reanalysis (JRA-55)<sup>47</sup>, and monthly ocean temperature from the Institute of Atmospheric Physics (IAP) ocean analysis are used to identify the mechanisms underlying the secular changes in TC intensity. We compute potential intensity (a theoretical maximum intensity that a TC can reach for a given SST and atmospheric thermodynamic profile<sup>48,49</sup>) following the work in ref.<sup>50</sup>. The upper-ocean thermal stratification is represented by the difference between ocean surface temperature and water temperature at a 75 m depth<sup>42</sup>, that is,  $SST - T_{75m}$ . We use the data averaged over July–October and January–April to represent the typical conditions during the TC peak season of the Northern Hemisphere and Southern Hemisphere, respectively. The linear trends in the large-scale atmospheric and oceanic variables during the period 1991–2020 are calculated by means of least-squares regression.

### Data availability

The 6-hourly positions and upper-ocean current velocities of drifters are obtained from <https://www.aoml.noaa.gov/phod/gdp/interpolated/data/all.php>. TC occurrence also with 6 h temporal resolution is acquired from the best track data from the Joint Typhoon Warning Center (<https://www.metoc.navy.mil/jtvc/jtvc.html?best-tracks>) for the Western Pacific Ocean, the Indian Ocean and the Southern Hemisphere, and the National Hurricane Center and Central Pacific Hurricane Center (<https://www.nhc.noaa.gov/data/#hudat>) for the Atlantic and Northeast and Central Pacific Oceans. Daily SST is from the NOAA 1/4° Optimum Interpolation Sea Surface Temperature (OISST), and it is downloaded from <https://www.ncei.noaa.gov/data/sea-surface-temperature-optimum-interpolation/v2.1/access/avhrr/>. The hourly current and wind data from the TAO/TRITON, RAMA and PIRATA buoy arrays are downloaded from <https://www.pmel.noaa.gov/tao/drupal/dissel/>. The JRA-55 Reanalysis dataset is downloaded from [https://jra.kishou.go.jp/JRA-55/index\\_en.html](https://jra.kishou.go.jp/JRA-55/index_en.html). The IAP monthly ocean temperature analysis data are downloaded from [ftp://www.ocean.iap.ac.cn/cheng/CZ16\\_y3\\_IAP\\_Temperature\\_gridded\\_1month.ncdf](ftp://www.ocean.iap.ac.cn/cheng/CZ16_y3_IAP_Temperature_gridded_1month.ncdf). Source data are provided with this paper.

# Article

## Code availability

Analysis and figure generation were performed using MATLAB. The code and scripts of the two main methods and four figures in the paper are available from Zenodo: <https://doi.org/10.5281/zenodo.7013352>.

43. Stewart, R. H. *Introduction to Physical Oceanography* (OAKTrust, 2008); <https://oaktrust.library.tamu.edu/handle/1969.1/160216>.
44. Hwang, P. A., Reul, N., Meissner, T. & Yueh, S. H. Whitecap and wind stress observations by microwave radiometers: global coverage and extreme conditions. *J. Phys. Oceanogr.* **49**, 2291–2307 (2019).
45. Zijlema, M., van Vledder, G. P. & Holthuijsen, L. H. Bottom friction and wind drag for wave models. *Coast. Eng.* **65**, 19–26 (2012).
46. Peduzzi, P., Concato, J., Kemper, E., Holford, T. R. & Feinstein, A. R. A simulation study of the number of events per variable in logistic regression analysis. *J. Clin. Epidemiol.* **49**, 1373–1379 (1996).
47. Kobayashi, S. et al. The JRA-55 Reanalysis: general specifications and basic characteristics. *J. Meteor. Soc. Japan.* **93**, 5–48 (2015).
48. Emanuel, K. A. The maximum intensity of hurricanes. *J. Atmos. Sci.* **45**, 1143–1155 (1988).

49. Holland, G. J. The maximum potential intensity of tropical cyclones. *J. Atmos. Sci.* **54**, 2519–2541 (1997).

50. Tang, B. & Emanuel, K. A ventilation index for tropical cyclones. *Bull. Amer. Meteor. Soc.* **93**, 1901–1912 (2012).

**Acknowledgements** G.W. and L.W. were supported by the National Key R&D Program of China (grant no. 2019YFC1510100) and the National Natural Science Foundation of China (grant no. 41976003).

**Author contributions** G.W. initiated the idea, designed the study and interpreted the results. L.W. processed the data and performed the analyses. All the authors developed the idea and wrote the paper. W.M. and S.-P.X. discussed the results and commented on the manuscript.

**Competing interests** The authors declare no competing interests.

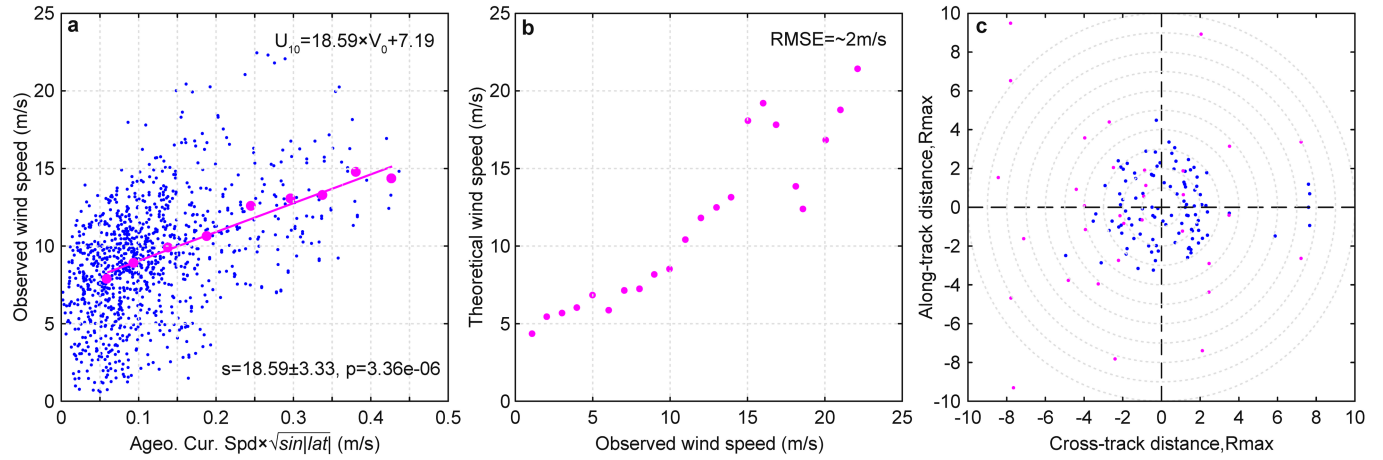
### Additional information

**Supplementary information** The online version contains supplementary material available at <https://doi.org/10.1038/s41586-022-05326-4>.

**Correspondence and requests for materials** should be addressed to Guihua Wang.

**Peer review information** *Nature* thanks the anonymous reviewers for their contribution to the peer review of this work. Peer reviewer reports are available.

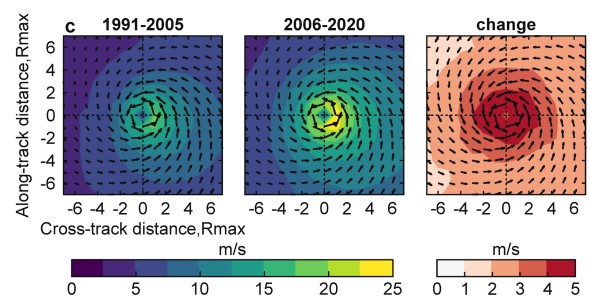
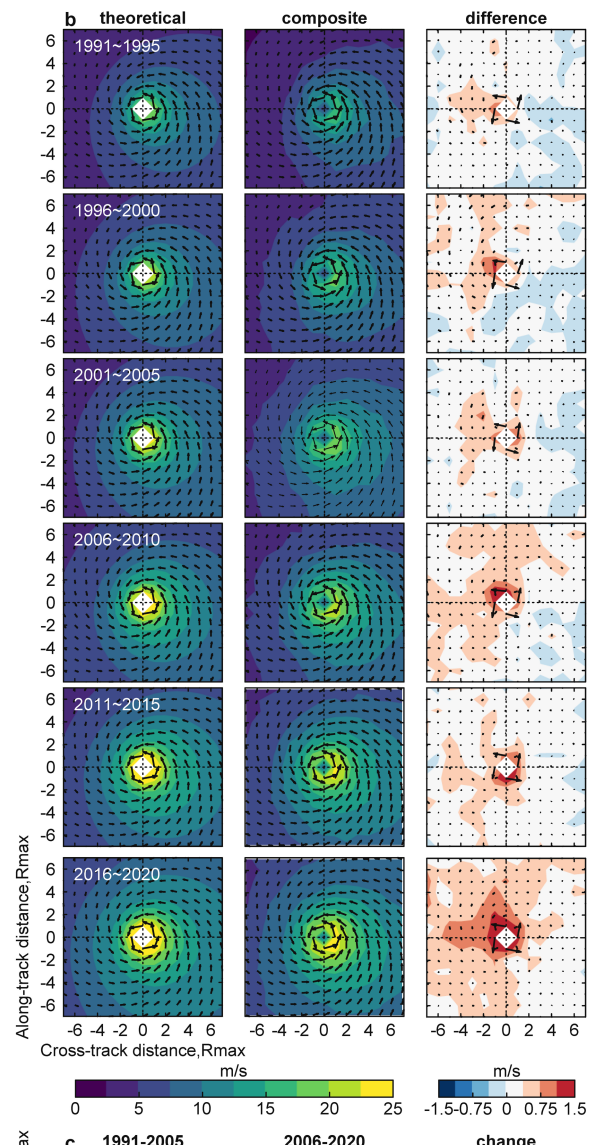
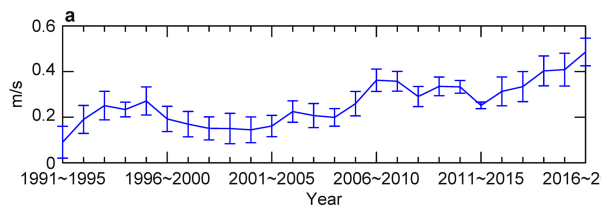
**Reprints and permissions information** is available at <http://www.nature.com/reprints>.



**Extended Data Fig. 1 | Buoy current and wind observations under TC conditions.** **a**, Relationship of observed wind speed and ageostrophic current speed considering latitudes under TC conditions (blue dots). Linear regression (red line) is also plotted between the binned averages of the observed wind speeds and current speeds (red dots), with  $V_0$  in the regression equation being coupling between the ageostrophic current speed  $V$  and latitude  $\varphi$  as  $V_0 = V \times \sqrt{\sin |\varphi|}$ , and the slope of the fitted line (along with the 95% margin of error and the p-value of the t-test) is reported in the bottom right corner. The binned averages of the current speeds are calculated from the ageostrophic current speeds in every  $0.1 \text{ m s}^{-1}$  bin, and the corresponding observed wind

speeds are taken to calculate the binned averages of the observed wind speeds. **b**, Comparison of the binned averages of the theoretical wind speeds estimated from the ageostrophic currents and observed wind speeds (red dots). The binned averages of the observed wind speeds are calculated from the observed wind speeds in every  $1 \text{ m s}^{-1}$  bin, and the corresponding theoretical wind speeds are taken to calculate the binned averages of the theoretical wind speeds. **c**, Distribution of buoys with current and wind observations in the TC-coordinate system (dots), with the purple dots indicating that the maximum wind speeds of the corresponding TCs are larger than 35 kt. The results are based on observations from the TAO/TRITON, RAMA, and PIRATA buoy arrays.

# Article



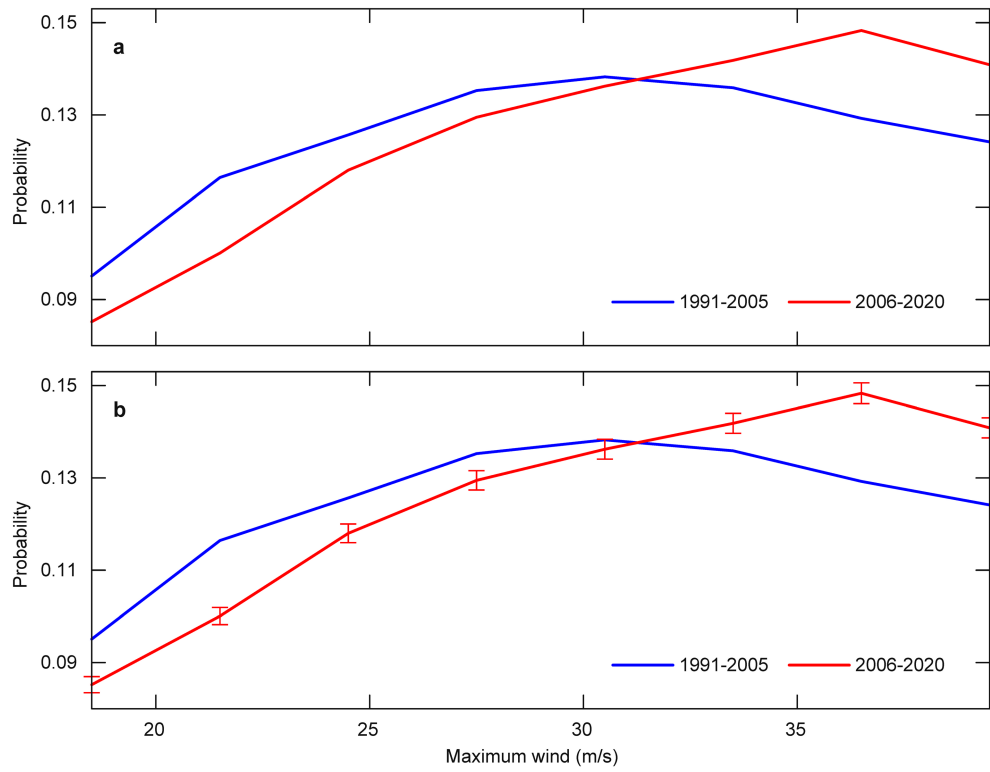
**Extended Data Fig. 2** | See next page for caption.

---

**Extended Data Fig. 2 | Winds of weak TCs derived from drifter current**

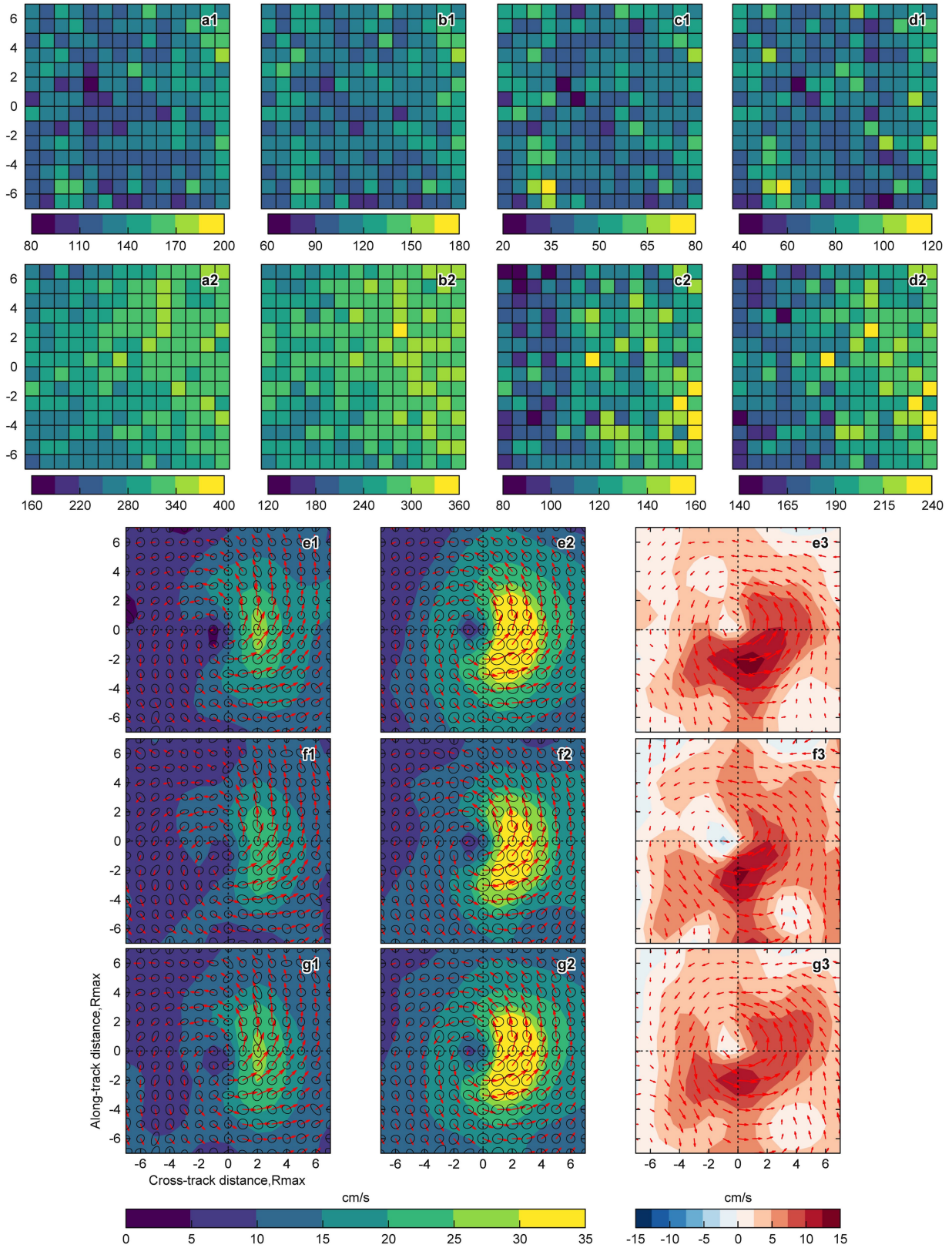
**measurements based on typhoon wind field model of Batts.** **a.** The difference of spatial averages between the theoretical wind fields and composite wind fields for each five-consecutive-year period from 1991 to 2020. The length of the error bar for each period is twice the standard deviation divided by the square root of the effective number of observations during that period (i.e., twice the standard error of the mean). The effective number of

observations is approximated as the number of observations that are separated by at least 500 km in distance or at least 10 days in time. **b.** The theoretical and composite wind fields for each five-consecutive-year period during 1991–2020, and differences between the two winds (theoretical winds minus composite winds). **c.** The composite wind fields for the periods of 1991–2005 and 2006–2020, and change of the wind fields between the two periods (2006–2020 minus 1991–2005).



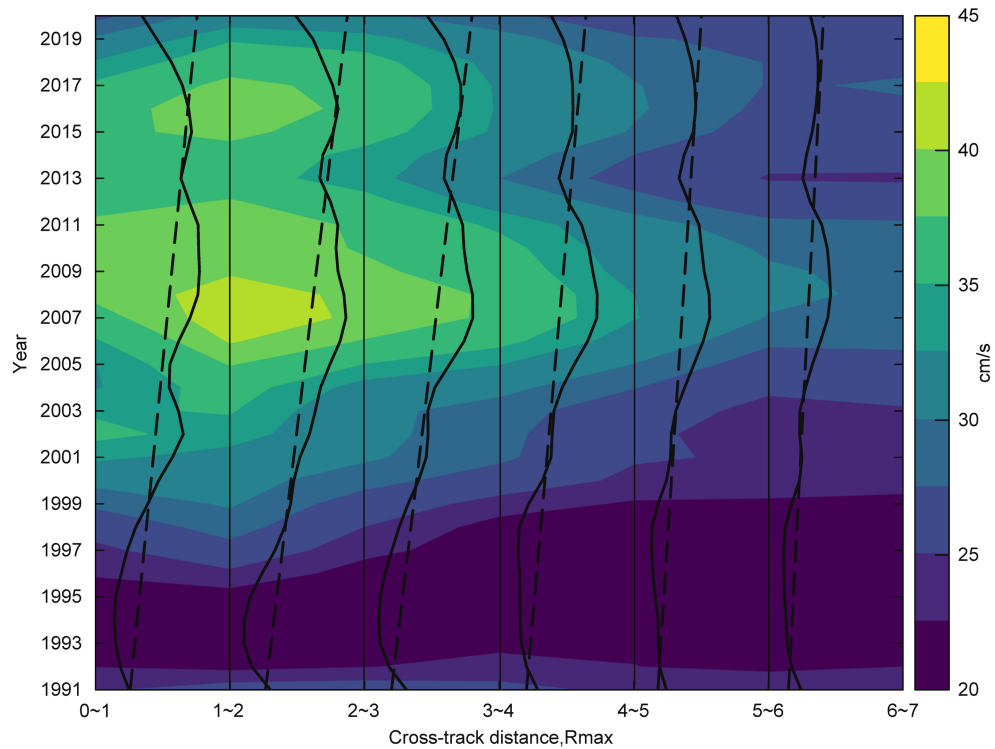
**Extended Data Fig. 3 | PDFs of the maximum sustained wind under global weak TCs.** for 1991–2005 (blue) and 2006–2020 (red) derived from (a) all drifter observations, and (b) the same as (a) but with the results for 2006–2020 obtained with a random sampling method. Specifically, the random sampling procedure was repeated 10,000 times. Each time, 25,538 observations (i.e., the

number available for the period of 1991–2005) were drawn from the entire 59,643 observations during 2006–2020, and a PDF of TC intensities was computed. The red curve shows the average PDF using the obtained 10,000 individual PDFs, with the error bars indicating the standard deviations of the 10,000 realizations. Bin size is  $3 \text{ m s}^{-1}$ .



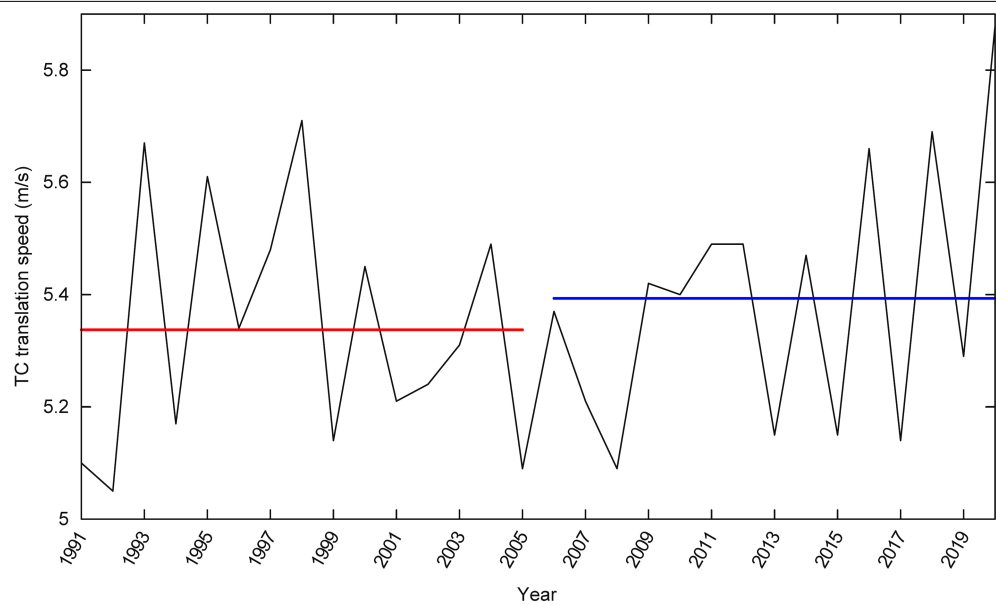
**Extended Data Fig. 4 | Drifter data quantity statistics and mean near-surface ocean current fields under weak TCs.** (a1, b1, c1, d1) are numbers of drifter records within  $r < 7R_{\max}$  for the period of 1991–2005, and (a2, b2, c2, d2) are the same as (a1, b1, c1, d1) but for 2006–2020, respectively. Global mean current fields, (e1, f1, g1) are for 1991–2005 and (e2, f2, g2) are for 2006–2020, and (e3, f3, g3) are changes of the mean currents between the two periods (2006–2020 minus 1991–2005). a1, a2 are for weak TCs range from 17 to 42  $\text{m s}^{-1}$ . b1, b2, e1–e3 are for weak TCs range from 17 to 32  $\text{m s}^{-1}$ , c1, c2, f1–f3 are for weak TCs whose LMI is 17 to 32  $\text{m s}^{-1}$ , d1, d2, g1–g3 are for weak TCs whose LMI is 17 to 42  $\text{m s}^{-1}$ , respectively.

2006–2020, and (e3, f3, g3) are changes of the mean currents between the two periods (2006–2020 minus 1991–2005). a1, a2 are for weak TCs range from 17 to 42  $\text{m s}^{-1}$ . b1, b2, e1–e3 are for weak TCs range from 17 to 32  $\text{m s}^{-1}$ , c1, c2, f1–f3 are for weak TCs whose LMI is 17 to 32  $\text{m s}^{-1}$ , d1, d2, g1–g3 are for weak TCs whose LMI is 17 to 42  $\text{m s}^{-1}$ , respectively.

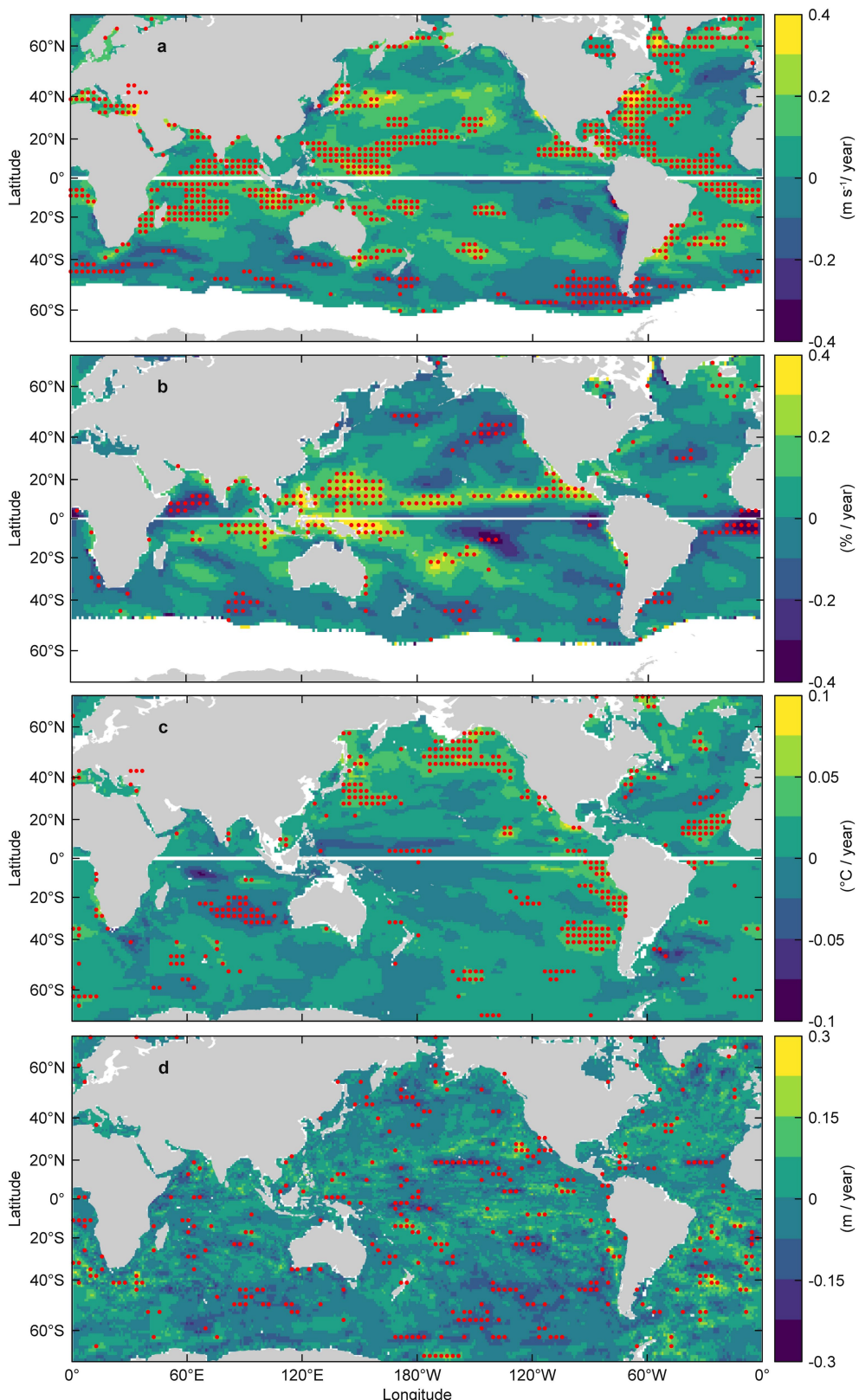


**Extended Data Fig. 5 | Evolution of the drifter measured ocean current speeds within  $r < 7R_{\max}$  under weak TCs.** from 1991 to 2020. The color shading and solid lines represent the current speeds at different distances from the

corresponding TC centers along the cross-track direction, and the dashed lines are the associated current speed trends. The lower and upper limits of all the lines are 18 and 45  $\text{cm s}^{-1}$ , respectively.



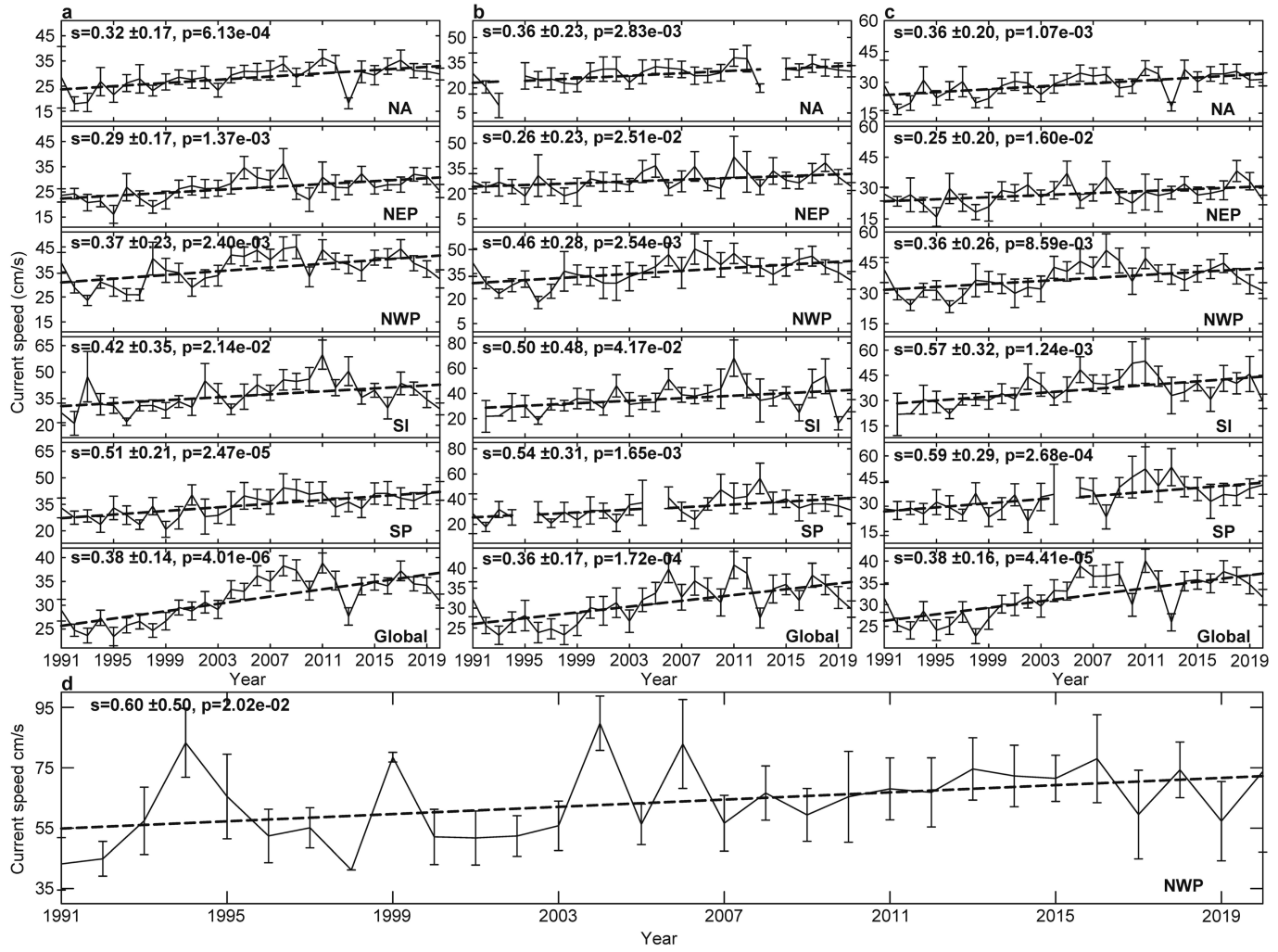
**Extended Data Fig. 6 | Translation speed ( $\text{m s}^{-1}$ ) of weak TCs during the period of 1991–2020.** The red and blue lines are the average during the periods of 1991–2005 and 2006–2020, respectively.



**Extended Data Fig. 7 | Linear trends in the large-scale atmospheric environment and upper-ocean thermal condition during 1991–2020.**

**a**, Potential intensity. **b**, Relative humidity at 600 hPa. **c**, Upper-ocean thermal stratification (represented by the difference of water temperature between ocean surface and 75-m depth, i.e.,  $\text{SST} - \text{T}_{75\text{m}}$ ). **d**, Mixed layer depth (MLD, depth

where the density change reaches a threshold value of  $0.03 \text{ kg m}^{-3}$  relative to the surface). The results in **a** and **b** are based on the JRA-55 reanalysis, and in **c** and **d** are calculated using the IAP ocean analysis data. Red dots denote regions where the linear trend is significant at the 0.05 level. Note this figure is produced by MATLAB.



**Extended Data Fig. 8 | Evolution of the near-surface ocean current speeds derived from drifters under TCs.** For individual basins and the globe. **a** is for weak TCs range from 17 to 32 m s<sup>-1</sup>, **b** is for weak TCs whose LMI is 17 to 32 m s<sup>-1</sup>, **c** is the same as **b** but LMI is 17 to 42 m s<sup>-1</sup>, and **d** is based on drifter data under strong TCs (Category-2–5) over NWP. The dashed lines indicate the fitted linear trends of the curves, and the estimated trends (along with the 95% margin of

errors) and the p-values of the t-test for the trends are also reported. In each panel, the length of the error bar for each year is twice the standard deviation divided by the square root of the effective number of observations in that year. Discontinuity points along the curves in **b** and **c** represent missing values due to insufficient data.

## Article

**Extended Data Table 1 | TC Intensity estimates by JTWC (Joint Typhoon Warning Center), JMA (Japan Meteorological Agency) and CMA (China Meteorological Agency)**

No.	TC number	UTC time	Latitude (°N)	Longitude (°E)	Vmax (m/s)
			JTWC / JMA / CMA	JTWC / JMA / CMA	JTWC / JMA / CMA
1	198304	1200/ 07/23/1983	18.2 / 18.1 / 18.1	127.6 / 127.6 / 127.6	41 / 33 / 65
2	198801	0600/ 01/17/1988	13.7 / 13.6 / 13.6	118.0 / 117.9 / 117.9	18 / 23 / 20
3	199001	0000/ 01/15/1990	15.5 / 15.5 / 15.5	145.8 / 145.8 / 145.8	39 / 28 / 35
4	200001	1800/ 05/09/2000	18.6 / 18.7 / 18.7	136.1 / 136.0 / 136.0	80 / 46 / 50
5	200302	0600/ 04/13/2003	10.2 / 10.1 / 10.2	149.8 / 149.8 / 149.9	33 / 28 / 30
6	200509	1200/ 08/05/2005	27.4 / 27.4 / 27.4	122.3 / 122.2 / 122.2	39 / 36 / 45
7	200519	0000/ 09/30/2005	22.0 / 22.0 / 22.0	132.1 / 132.1 / 132.1	64 / 41 / 45
8	200705	1800/ 07/29/2007	18.7 / 18.7 / 18.7	143.3 / 143.3 / 143.3	33 / 23 / 28
9	201501	1800/ 01/17/2015	12.7 / 12.7 / 12.7	124.2 / 124.3 / 124.3	26 / 21 / 23
10	201502	0600/ 02/10/2015	14.2 / 14.2 / 14.2	154.2 / 154.2 / 154.2	67 / 46 / 48

**Extended Data Table 2 | Trends in drifter-measured ocean current speeds within varying  $R_{\max}$  of weak TCs during the period of 1991–2020**

Basin	$R_{\max}$						
	1	2	3	4	5	6	7
global	0.50±0.27	0.71±0.24	0.65±0.20	0.58±0.20	0.51±0.18	0.45±0.16	0.40±0.15
NA	0.21±0.38	0.48±0.26	0.47±0.22	0.46±0.21	0.42±0.20	0.40±0.18	0.35±0.18
NEP	0.48±0.49	0.52±0.49	0.58±0.34	0.52±0.28	0.40±0.22	0.32±0.19	0.29±0.16
NWP	0.88±0.45	0.71±0.40	0.52±0.38	0.49±0.33	0.45±0.29	0.41±0.26	0.36±0.23
SI	0.41±0.85	0.71±0.71	0.64±0.60	0.52±0.57	0.48±0.47	0.40±0.40	0.39±0.34
SP	0.64±0.86	0.99±0.72	0.80±0.52	0.81±0.36	0.65±0.28	0.59±0.24	0.54±0.23

All units are  $\text{cm s}^{-1}$  per year. The trend is tabulated along with the corresponding 95% margin of error.